Atmospheric
Measurement
Techniques

Comparison of the cloud top heights retrieved from MODIS and AHI satellite data with ground-based Ka-band radar

Juan Huo, Daren Lu, Shu Duan, Yongheng Bi, and Bo Liu

Key Laboratory for Atmosphere and Global Environment Observation, Chinese Academy of Sciences, Bejing, 100029, China

Correspondence: Juan Huo (huojuan@mail.iap.ac.cn)

Abstract. To better understand the accuracy of cloud top heights (CTHs) derived from passive satellite data, ground-based Ka-band radar measurements from 2016 and 2017 in Beijing are compared with CTH data inferred from the Moderate Resolution Imaging Spectroradiometer (MODIS) and the Advanced Himawari Imager (AHI). Relative to the radar CTHs, the MODIS CTHs are found to be underestimated by -1.10 ± 2.53 km on average and 49 % of CTH differences are within 1.0 km. The AHI CTHs are underestimated by -1.10 ± 2.27 km and 42 % are within 1.0 km. Both the MODIS and AHI CTH retrieval accuracy depends strongly on the cloud depth (CD). Large differences are mainly due to the retrieval of thin clouds of CD < 1 km, especially when the cloud base height is higher than 4 km. For clouds with CD > 1 km, the mean CTH difference decreases to -0.48 ± 1.70 km for MODIS and to -0.76 ± 1.63 km for AHI. It is found that MODIS CTHs with higher values (i.e. > 6 km) show smaller discrepancy with radar CTH than those MODIS CTHs with lower values (i.e. < 4 km). Statistical analysis illustrate that the CTH difference between the two satellite instruments is lower than the difference between the satellite instrument and the ground-based Ka-band radar. The monthly accuracy of both CTH retrieval algorithms is investigated and it is found that summer has the smallest retrieval difference.

1 Introduction

Clouds play important role in the water and energy budgets in the Earth–atmosphere system (Ramanathan et al., 1989; Liou, 1992; Cess et al., 1996; Boucher et al., 2013). They are one of the least understood components, and also one of the largest uncertainty sources, in general circulation model (GCM) simulations (Wetherald and Manabe, 1988; Arakawa, 2004). Cloud top height (CTH) is one of the important cloud parameters that provide information about the vertical structure of cloud water content (Stubenrauch et al., 1997; Marchand et al., 2010). Cloud vertical distributions determine diabatic heating profiles. Comparisons of stratocumulus CTHs simulated from GCMs with those retrieved from satellites suggested that either satellite retrievals placed stratocumulus clouds too high in the atmosphere or GCM cloud tops were biased too low (Rossow and Schiffer, 1999). Knowledge of CTH is crucial to understanding the Earth's radiation budget and global climate change.

Active and passive instruments have long been used for monitoring CTHs (Atlas, 1954; Schiffer and Rossow, 1983; Pavolonis and Heidinger, 2004; Stephens and Kummerow 2007; Huo and Lu 2009; Görsdorf et al., 2015). Active instruments, i.e. cloud radars and lidars, detect CTH directly through reflectivity from cloud top particles. Passive infrared (IR) instruments measure the IR brightness temperature of the cloud to derive CTH based on assumptions, for instance, that an opaque cloud could be regarded as a black body. Surface measurements and satellite measurements have individual strengths and weaknesses. Some active instruments, i.e. radar, are ideal sensors for accurately detecting the CTH. Yet, surface instruments are limited in spatial scale. Satellites measure large-scale cloud systems, but the CTHs retrieved from passive IR instruments are still subject to large uncertainties. This study assesses the accuracy of the CTHs derived from passive satellites through comparison with surface active radar data.

The Moderate Resolution Imaging Spectroradiometer (MODIS) on board the Aqua and Terra satellites has been in service since 2000 and its cloud products are being widely used by the meteorological community (King et al., 1998; Ackerman, 1998; Rodell and Houser, 2004; Roskovensky and Liou, 2006; Remer et al., 2008; Pincus et al., 2012). Uncertainties in the MODIS CTH products have been assessed using many measurements, i.e. from the ground, aircraft and satellites (Naud et al., 2002; Weisz et al., 2007; Ham et al., 2009; Chang et al., 2010; Marchand et al., 2010; Baum et al., 2012; Marchand, 2013; Xi et al., 2014; Håkansson et al., 2018; Wang et al., 2019). Naud et al. (2002) showed that the two sets of averaged CTHs from the Multi-Angle Imaging Spectroradiometer (MISR) and MODIS were generally within 2 km of each other over the British Isles. Holz et al. (2008) found that MODIS underestimated the CTH relative to the Cloud-Aerosol Lidar with Orthogonal Polarization (CALIOP) by 1.4 ± 2.9 km globally over a 2 month period. Xi et al. (2014) found that daytime CTH of marine boundary layer cloud retrieved from MODIS was 0.063 km higher on average than what surface lidar and radar had measured. Håkansson et al. (2018) used global collection 6 MODIS cloud top products to compare with CloudSat cloud profiling radar data and reported that the mean difference was -0.61 ± 2.53 km. Previous global evaluation results might be different to the specific regions. This study compares the retrieved MODIS CTHs with radar measurements in Beijing over a long period and provides further knowledge about the uncertainty of MODIS CTH products.

The Advanced Himawari Imager (AHI) on board the Himawari-8 (HW8) satellite, a geostationary meteorological satellite, has provided CTHs since July 2015 (Bessho et al., 2016). Zhou et al. (2019) reported that the CTHs derived from surface Ka-band radar from December 2016 to November 2017 were 0.82 km higher than the retrieved CTH from the AHI radiance data using a Fengyun Geostationary Algorithm Testbed-Imager (FYGAT-I) science product algorithm. Mouri et al. (2016) reported that the mean AHI CTH was lower than the MODIS and CALIOP CTH over 2 weeks of measurements. The AHI CTH retrievals are relatively new to the meteorological community and require further evaluation before application in meteorological studies.

MODIS and AHI share some common principles and technologies used for the CTH retrieval. However, the specific retrieval algorithms are different in terms of the radiative transfer model, atmospheric profiles, source measurements and cloud types. A Ka-band (35.075 GHz) radar at the Institute of Atmospheric Physics in Beijing, China ($39.96°$ N, $116.37°$ E), has been used for cloud measurements since 2012 (Huo et al., 2019). In this study, we compare and evaluate the CTHs retrieved from the passive satellite instruments on board a polar-orbiting satellite and a geostationary satellite with those measured by a surface active radar in Beijing over a long period. To our knowledge, this study presents the first comparison and evaluation of the CTH datasets for Bei-

jing from MODIS and AHI. This work quantifies the satellite CTH retrieval accuracy and provides a reference and usage guidance for the application of the CTH datasets in meteorological research, such as climate model simulations for Beijing and northern China.

2 Description of the MODIS, AHI and Ka-band radar CTH retrievals

2.1 MODIS CTH retrieval

MODIS measures radiance in 36 spectral bands from 0.42 to 14.24 µm at three spatial resolutions: 250, 500 and 1000 m. The swath dimensions are 2330 km (cross-track) by 10 km (along-track at nadir). MODIS cloud top pressure (height) is determined by a combination algorithm of CO_2-slicing technology (also known as the radiance ratioing technology) and infrared window technology (IRW, using the 11 µm brightness temperature, Smith and Platt, 1978; Nieman et al., 1993) in conjunction with the National Center for Environmental Prediction Global Data Assimilation System temperature profiles (Menzel et al., 2008; Baum et al., 2012). Equations (1)–(3) below present the basic theory of the CO_2-slicing technology for which Menzel et al. (2008) presented thorough descriptions.

$$R(v) = (1 - NE) R_{clr}(v) + NE[R_{bcd}(v, P_c)] \tag{1}$$

$$R_{bcd}(v, P_c) = R_{clr}(v) \int_{P_c}^{P_s} \tau(v, p) \frac{dB[v, T(p)]}{dp} dp \tag{2}$$

$$\frac{R(v1) - R_{clr}(v1)}{R(v2) - R_{clr}(v2)} = \frac{NE1 \int_{P_s}^{P_c} \tau(v1, p) \frac{dB[v1, T(p)]}{dp} dp}{NE2 \int_{P_s}^{P_c} \tau(v2, p) \frac{dB[v2, T(p)]}{dp} dp} \tag{3}$$

Here v is the frequency, E is the emissivity of cloud, $R(v)$ is the measured radiance, R_{clr} is the radiance of clear sky and R_{bcd} is the radiance of black body. N is the cloud coverage of the field of view in the range of $0 \sim 1$, $\tau(v, p)$ is the fractional transmittance of radiation at the wavelength v from the atmospheric pressure level (p) arriving at the top of the atmosphere ($p = 0$), P_c is the cloud top pressure, $B[v, T(p)]$ is the Planck radiance at the wavelength v at the temperature $T(p)$ and P_s is the surface pressure. The CO_2-slicing technology assumes the emissivity of the cloud to be the same at two close wavelengths, which is nearly correct for ice clouds but less so for water clouds.

For the CO_2-slicing technology, Terra-MODIS CTHs are retrieved based on the channels 36/35 and 35/33 (corresponding to 14.2/13.94 and 13.94/13.34 µm) ratio pairs due to noise problems at band 34. Aqua-MODIS CTHs are retrieved by the following three ratio pairs: channels 36/35, channels 35/34, channels 34/33 (14.2/13.94, 13.94/13.64, 13.64/13.34 µm). In the collection 5 version algorithm, when the radiance difference between cloud and clear sky is so

Figure 1. The Ka-band polarization Doppler radar at the Institute of Atmospheric Physics, Chinese Academy of Sciences, Beijing, China (39.967° N, 116.367° E).

Table 1. Main technical specifications of the Ka radar at the IAP.

	Parameters	Technical specification
Transmitter	Frequency	35.075 GHz
	Peak power	29 kW
	Pulse width	0.2 µs
	Type	Magnetron
	Pulse repetition frequency	3.5 kHz
Antenna	Diameter	1.5 m
	Gain	54 dB
	Scanning mode	Vertically pointing
	Beam width	0.4°
Receiver	Noise	5.8 dB
	Noise power	−103 dBm
	Vertical resolution	30 m

small that CO_2-slicing technology is unsuitable for CTH retrieval, the IRW is applied. Compared with the collection 5 version algorithm, collection 6 differs in terms of the spatial resolution and the radiative transfer model calculation, for example, using ozone profiles provided in the meteorological products rather than from climatological values. Furthermore, application of the CO_2-slicing method is limited to only ice cloud in collection 6 (Baum et al., 2012). The MODIS cloud products used in this study are the collection 6 version cloud datasets (MYD06/MOD06) from both Aqua and Terra at 1 km spatial resolution.

2.2 AHI CTH retrieval

The HW8 satellite, equipped with the AHI, was launched on 7 October 2014 at the location of 140.7° E and its operation by the Japanese Meteorological Agency commenced on 7 July 2015 (Bessho et al., 2016). The AHI is a visible infrared radiometer that has 16 observation bands, ranging from 0.47 to 13.3 µm (3 for visible, 3 for near-infrared and 10 for infrared). The AHI observes the Japanese area and some other target or landmark areas every 2.5 min and the entire full disk every 10 min with a spatial resolution of 0.5–2.0 km. The scan ranges for full disk and the Japanese area are preliminarily fixed, while those for the target and landmark areas are flexible regarding meteorological conditions. Relative to the imagers on board previous Japanese geosta-

tionary satellites, the AHI is improved in terms of its number of bands, spatial resolution, temporal frequency and radiometric calibration.

The AHI CTH retrieval algorithm uses radiative transfer codes (Eyre, 1991) developed by EUMETSAT and numerical weather prediction temperature and humidity profile data to calculate the radiance of four infrared bands (wavelengths 6.2, 7.3, 11.2 and 13.3 µm). It involves the interpolation method, the CO_2-slicing method and the intercept method. The selection of method depends on the cloud type from AHI cloud type product (Neiman et al., 1993; Schmetz et al., 1993; Mouri et al., 2016). The interpolation method is similar to the IRW. The vertical profile of radiance at 11.2 µm is calculated using radiative transfer codes and compared with the radiance observed by AHI. Cloud top height is then determined from the interpolation ratio of radiance between two levels sandwiching the observed radiance. The interpolation method is adopted for opaque and fractional cloud. The intercept method uses three scatter plots of observed radiances (containing 33×33 pixels around the target pixel) at two band pairs (11.2/6.2, 11.2/7.3 and 11.2/13.3 µm) and the calculated black body radiance curve to determine cloud top height (which has the minimum pressure) from the intersection. The intercept method is used for semi-transparent cloud. In the retrieval process for optically thin (or semi-transparent) clouds, if the intercept method does not produce suitable results, the CO_2-slicing method is applied. If this also fails to produce suitable results, the interpolation method is utilized. The AHI cloud products used in this study are the Himawari-8 Cloud Property data released through the JAXA's P-Tree System (https://www.eorc.jaxa.jp/ptree/index.html, last access: 16 September 2019).

2.3 Ka-band radar

The Ka-band polarization Doppler radar using a wavelength of 8.55 mm (Ka radar), situated at the Institute of Atmospheric Physics (IAP, 39.967° N, 116.367° E), Beijing, China, was set up in 2010 (Fig. 1). The technical specifications of the Ka-band radar are given in Table 1. The Ka radar works $24\,h\,d^{-1}$ in a vertically pointing mode, except during special events, such as heavy rain or short-term collaborative observations with other instruments, when the mode is changed.

A data quality control approach using a combination of the threshold and median filter methods has been implemented to reduce the effects of clutter and noise on the radar reflectivity (Xiao et al., 2018). It is considered to be cloudy if the reflectivity profile contains more than three bins of radar reflectivity data higher than $-45\,dBZ$. Zhou et al. (2019) used a threshold of $-40\,dBZ$ for cloud determination because their Ka radar was equipped with an all-solid transmitter that was different to our Ka radar. A higher threshold might miss some clouds with weak returns.

For a cloudy profile, the CTH is determined as the height of the cloudy bin at the highest level. In order to compare with passive satellite data, for clouds detected in a period (i.e. within 10 min), the radar CTH is calculated as the mean CTH of all cloudy profiles but not upper-level cloud if there are multilayer clouds. Note that the radar CTH differs when the upper-level cloud partially but not completely covers low-level cloud (see Fig. 2). For a cloudy profile, the cloud base height (CBH) is determined by the lowest cloudy radar bin. The cloud depth (CD) is equal to the CTH minus the CBH. The final CBH (or CD) is the average value of all CBHs (or CDs).

3 Comparison scheme

A MODIS or AHI CTH pixel covers a larger area than a single profile of radar. The data repetition frequency also differs. Temporal and spatial collocation of the radar, MODIS and AHI data is critical to facilitate effective comparison and evaluation.

3.1 Collocation of the MODIS and Ka radar

A MODIS CTH pixel at sub-satellite point covers an area of about $1\,km^2$; vertically pointed radar takes about 1.7 min to scan a 1 km path and about 8 min for a 5 km path if the moving speed of cloud is $10\,m \times s^{-1}$. If the moving speed becomes higher (or lower), the required time scanning the same path will decrease (or increase). To compensate for the temporal and spatial differences in satellite data and ground-based data, Naud and Muller (2002) used MODIS CTH data averaged over a ± 0.1 latitude–longitude box for comparison with surface radar data. Dong et al. (2008) used the surface data (on the southern Great Plains, SGP, USA, atmospheric
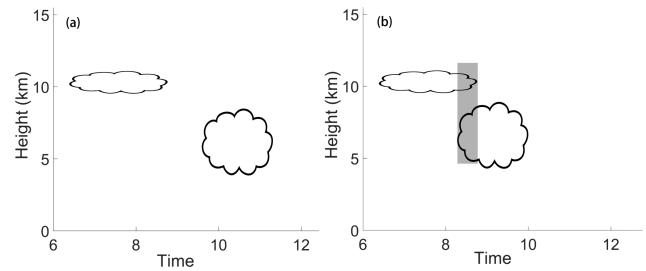
Figure 2. When multilayer clouds exist, the radar CTH is the mean CTH of all cloudy profiles but not upper-level cloud if **(a)** upper-level cloud and low-level cloud is situated separately or if **(b)** upper-level cloud covers part of the low-level cloud. The CTH of the grey "covered" part of low-level cloud is not considered.

observatory established by the Atmospheric Radiation Measurement, ARM) averaged over a 1 h interval and the satellite data averaged within a $30\,km \times 30\,km$ area for the surface–satellite comparison. In Holz et al. (2008), the 5 km averaged CALIOP data were collocated with the 1 km MODIS data. These collocation methods are designed to satisfy different instrument and observation conditions.

At the IAP site, a collocation scheme is determined according to the local conditions. The moving speed and direction of cloud is always changing, resulting in variable radar scanning length. The MODIS 1 km spatial resolution is suitable for pixels around the sub-satellite point, but those pixels around the IAP site have flexible spatial resolutions due to the viewing geometry of the individual satellite overpasses (see Fig. 3).

In this study, the ground-based CTH measurements from radar are averaged within 10 min of the MODIS overpass (MODIS observation time ± 5 min). All the MODIS CTHs within 5 km to the IAP site are extracted and averaged to compare with surface radar measurements. A detailed description of the investigation of the optimal collocation scheme, including comparison between collocations using 4 years of MODIS and radar data averaged over different times and areas, will take place in an additional analysis but is briefly discussed here. Figure 4 presents the statistical results from four collocation methods: radar data averaged within 5 min vs. nearest MODIS (D_{m0-r5}), radar within 5 min vs. MODIS averaged over a 5 km radius (D_{m5-r5}), radar within 5 min vs. MODIS within 30 km (D_{m5-r30}) and radar within 30 min vs. MODIS within 30 km ($D_{m30-r30}$). It is found that the D_{m5-r5} is close to the average of four collocation methods.

3.2 Collocation of the AHI and Ka radar

Due to the Himawari-8 viewing geometry, an AHI CTH pixel has a fixed $5\,km \times 5\,km$ spatial resolution and 10 min temporal resolution over the IAP site (Fig. 5). Since the AHI presents data every 10 min, the Ka radar data within
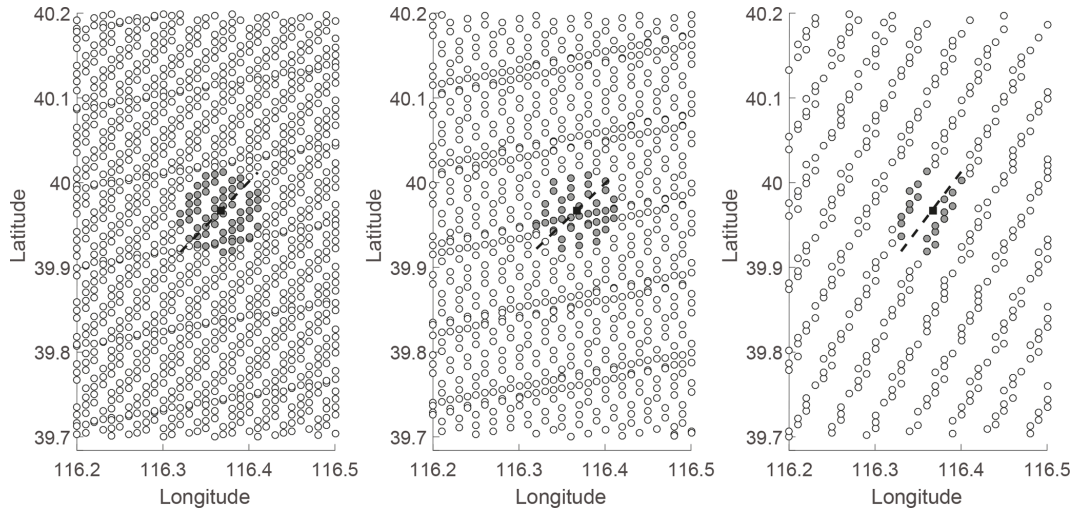
Figure 3. Locations of the Terra MODIS CTHs (circles) and the Ka radar (solid black squares). The three panels exhibit three spatial resolutions of MODIS CTH data due to the changing viewing geometry of the individual satellite overpass. Solid grey circles are MODIS pixels within 5 km of the IAP site. The possible path scanned by Ka radar is demonstrated by a dashed black line.
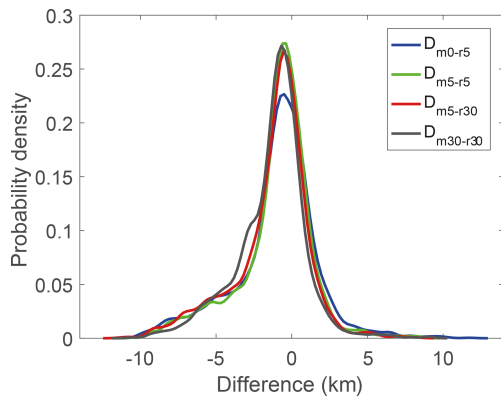
Figure 4. Distributions of the probability density of the CTH difference (MODIS – radar) from four collocation methods. D_{m0-r5}: radar data averaged within 5 min vs. nearest MODIS; D_{m5-r5}: radar 5 min vs. MODIS averaged within 5 km; D_{m5-r30}: radar 5 min vs. MODIS 30 km; and $D_{m30-r30}$: radar 30 min vs. MODIS 30 km.

Figure 5. Locations of the AHI CTHs (circles) and the IAP Ka radar (solid black dots). The spatial resolution of the AHI CTH data of the full disk does not change.

10 min of the AHI observation time are extracted and averaged (±5 min). The AHI CTHs nearest to the IAP site are used for comparison.

4 Comparison results

In this study, the CTH difference (D_{mr}) between the radar and MODIS data, the CTH difference (D_{ar}) between the radar and AHI data, and the CTH difference (D_{am}) between the AHI and MODIS data are defined as follows:

$$D_{mr} = H_m - H_r, \quad (4)$$
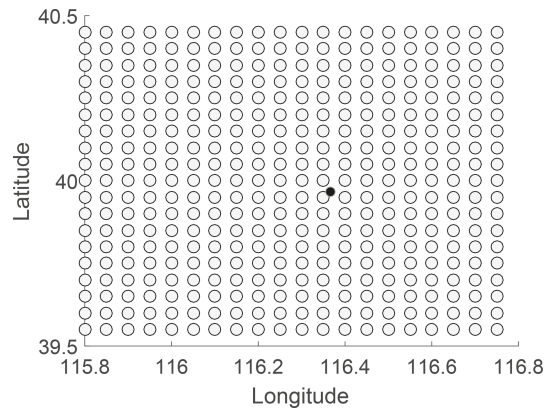$$D_{ar} = H_a - H_r, \quad (5)$$
$$D_{am} = H_a - H_m, \quad (6)$$

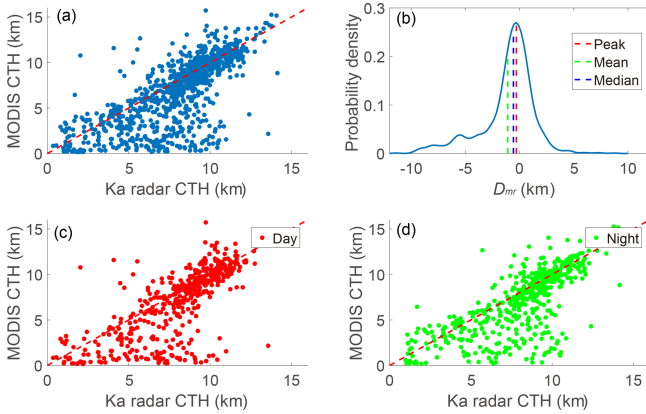where H_r is the radar CTH, H_m is the MODIS CTH and H_a is the AHI CTH.

This study uses the radar and satellite data observed from 1 January 2016 to 31 December 2017 for comparison purposes.

4.1 Comparison between MODIS and Ka radar

After discarding clear-sky data, Ka radar and MODIS have 963 valid CTH comparison pairs from 1 January 2016 to 31 December 2017 (Fig. 6a). The correlation coefficient

Figure 6. Scatter plot of MODIS CTHs and the Ka radar CTHs from **(a)** all comparisons, **(c)** comparisons at daytime and **(d)** comparisons at night-time. Panel **(b)** shows the probability density distribution of the D_{mr}, and the peak, mean and median difference is illustrated with dashed red, green and blue lines, respectively.
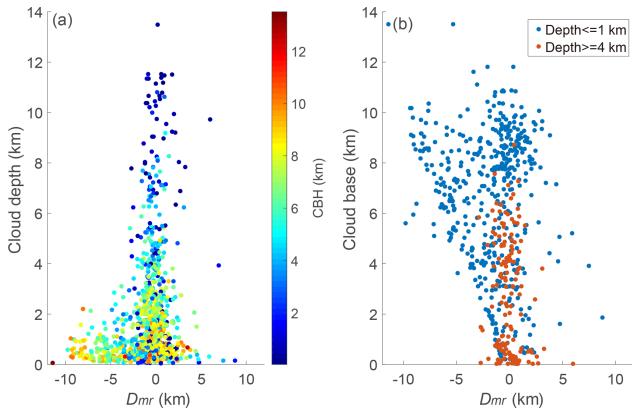
Figure 7. The relationship between **(a)** the D_{mr} and cloud depth and **(b)** the D_{mr} and the cloud base height (CBH) in cases of cloud depths $<= 1$ km (blue) and $>=4$ km.

between MODIS CTHs and radar CTHs is 0.72, which show a good agreement with each other. Relative to the Ka radar, MODIS tends to underestimate the CTHs, by -1.10 ± 2.53 km (mean $\pm$ standard deviation, STD, of the D_{mr}) on average. Among all comparisons, about 14 % of differences are within ±0.25 km, 27 % are within ±0.5 km and 49 % are within ±1.0 km. The statistical result is very close to the global results reported by Håkansson et al. (2018). Figure 6b presents the probability density distribution of the D_{mr} but the peak is not centred at zero. Most previous comparison studies used the mean bias to describe the CTH difference (Naud et al., 2002; Holz et al., 2008; Chang et al., 2010; Xi et al., 2014). Håkansson et al. (2018) discussed which statistical method was appropriate for describing a non-Gaussian distribution of CTH difference and found the median was better than the mean to describe the tendency. Here, in Fig. 6b, the peak is at -0.30 km (termed "peak" difference) and the me-
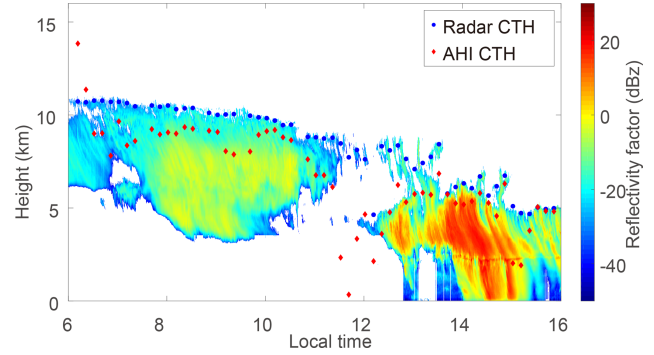

Figure 8. Examples of the Ka radar CTHs (blue dots) and the AHI CTHs (red diamonds) measured on 9 May 2016 from 06:00 to 16:00 (local time: UTC +8).

dian is at -0.57 km with 2.18 km IQR (interquartile range). It is clear that the median difference is closer to the peak difference than the mean difference. In this paper, both mean and median differences are used to describe the CTH difference.

From Fig. 6a, it can be seen that most large-underestimated matches have lower MODIS CTHs, i.e. lower than 4 km. Among all MODIS CTHs, 62 % are greater than 6 km, of which the mean D_{mr} is 0.0026 ± 1.43 km; yet, the mean D_{mr} is -3.55 ± 2.99 km when the MODIS CTHs are less than 4 km. When compared with lower MODIS CTHs, MODIS CTHs greater than 6 km show better agreement with the Ka radar data. That is, a MODIS CTH greater than 6 km is more likely to be close to radar CTH than a MODIS CTH less than 4 km. Comparisons between day and night show that the mean D_{mr} values during the day and night are close to each other (Fig. 6c, d). Terra MODIS and Aqua MODIS show similar accuracy in the CTH retrieval over Beijing.

Uncertainties in the MODIS CTH retrieval depend strongly on cloud depth (Fig. 7a). When cloud becomes thicker, the range of D_{mr} narrows gradually toward zero. Furthermore, the absolute D_{mr} decreases with increasing CD (Table 2). Large differences are mainly due to thin clouds (CD < 1 km). For clouds with CD > 1 km, the mean D_{mr} is -0.48 ± 1.70 km and the median (IQR) is -0.32 (1.42) km; the mean D_{mr} is -0.29 ± 1.43 km and median (IQR) is -0.29 (0.32) km for CD > 2 km. Figure 7b shows that the D_{mr} changes within small range as the CBH increases when the CD is greater than 4 km. It means that there is no obvious relationship between D_{mr} and CBH for thick clouds. However, for thin clouds of CD < 1 km, MODIS tends to greatly underestimate the CTH of high-level clouds, especially for the clouds with CBH > 4 km. Clouds with CBH > 4 km and CD < 1 km account for 37 % of all comparisons, and the mean D_{mr} is -2.16 ± 3.17 km. Clouds of CBH < 4 km and CD < 1 km account for 10 % of all cases, and the mean D_{mr} is -0.37 ± 2.07 km. Here it is found that the MODIS retrieval algorithm shows large uncertainties for high and thin clouds; i.e. CBH is > 4 km and CD is < 1 km.
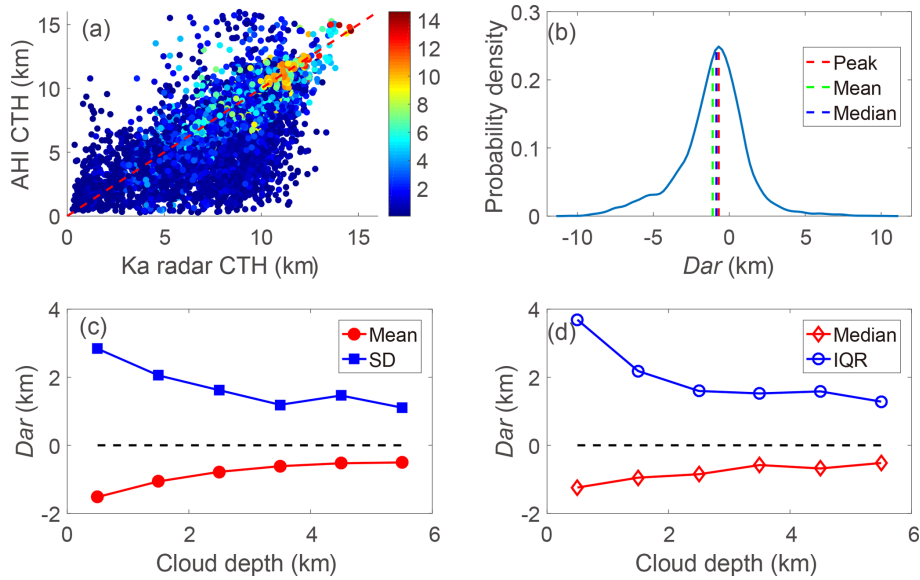
Figure 9. Statistical results of comparisons between Ka radar and AHI. Panel **(a)** shows the Ka radar CTHs and the AHI CTHs of all comparisons. Panel **(b)** is the same as Fig. 6b but for the D_{ar}. **(c)** The mean D_{ar} and the STD changes with CD. **(d)** The median of D_{ar} and IQR changes with CD.

Table 2. The median (IQR), mean and standard deviation of D_{mr} with different CDs (mean $\pm$ STD) (unit: km).

CD	$\in (0,1)$	$\in (1,2)$	$\in (2,3)$	$\in (3,4)$	$\in (4,5)$	> 5
Median (IQR)	-1.14 (3.79)	-0.45 (1.70)	-0.45 (1.38)	-0.28 (1.23)	-0.06 (1.02)	-0.24 (1.43)
Mean $\pm$ STD	-1.74 ± 3.04	-0.91 ± 2.17	-0.60 ± 1.61	-0.18 ± 1.45	-0.24 ± 1.00	0.01 ± 1.30

Among all 963 comparisons, 753 comparisons have only one cloud layer. For single-layer clouds, the mean D_{mr} is -1.06 ± 2.39 km and the median (IQR) is -0.55 (1.99) km, while the mean D_{mr} is -1.23 ± 2.98 km and the median (IQR) is -0.70 (2.72) km for multilayer clouds. Cloud occurrence frequency (COF) is equal to the number of radar cloudy profiles divided by the total number of radar profiles. It is found that the mean D_{mr} declines to -0.39 ± 1.57 km for the comparisons when the CD was > 1 km and the COF is > 0.5. Here, the MODIS retrieval algorithm shows higher accuracy for continuous clouds than for broken clouds.

4.2 Comparison between AHI and Ka radar

Figure 8 shows CTHs from the Ka radar and AHI over 10 h on 9 May 2016. Relative to the comparisons between MODIS and Ka radar, the number of comparisons between the Ka radar and AHI increases due to the increase in temporal resolution of the data. From 1 January 2016 to 31 December 2017, 6719 valid comparisons are found for the CTH comparison.

It can be seen from Fig. 8 that most AHI CTHs are lower than the radar CTHs. All of the 6719 CTH comparisons are shown in Fig. 9a.
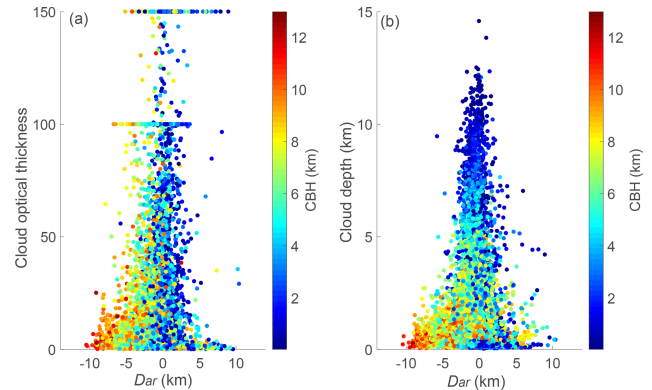
Figure 10. Scatter plot illustrating the relationship of **(a)** the D_{ar} and the COTs and **(b)** the D_{ar} and the CD.

Statistically, the mean D_{ar} is -1.10 ± 2.27 km, the median D_{ar} is -0.85 km with an IQR of 2.32 km, and the peak is at -0.70 km (Fig. 9b). About 11 % of the differences are less than 0.25 km, 22 % are within 0.5 km and 42 % are within 1.0 km. The mean D_{ar} is close to the mean D_{mr}. The standard deviation is lower due to more comparisons being available. However, the median D_{ar} and "peak" D_{ar} is lower than the median D_{mr} and peak D_{mr}, respectively.

Table 3. Statistical results of the distribution of D_{mr}, D_{ar} and D_{am} (unit: km).

	Mean	Median	Peak	STD	IQR
D_{mr}	−1.1	−0.57	−0.3	2.53	2.18
D_{ar}	−1.1	−0.85	−0.7	2.27	2.32
D_{am}	−0.64	−0.43	−0.18	2.36	1.93

Cloud depth is also a critical factor impacting the accuracy of the AHI retrieval algorithm (Fig. 9c, d). The mean D_{ar} decreases as the CD increases, i.e. the mean D_{ar} is -1.52 ± 2.84 for CD < 1 km while the D_{ar} declines to -0.76 ± 1.63 km for CD > 1 km. The AHI CTHs illustrate great variation for thin clouds (CD < 1 km). The mean bias is larger than the median bias when CD < 2 km. The relationship between the D_{ar} and the cloud optical thickness (COT) is compared with that between the D_{ar} and CD (Fig. 10). All COTs are from AHI cloud products. The range of the D_{ar} narrows as the COT increases, but the distribution is much more scattered than that for CD, which might be due to the COT retrieval errors.

Among all comparisons, 79 % have only one cloud layer. For single-layer clouds, the mean D_{ar} is -1.12 ± 2.25 km and the median D_{ar} is -0.88 km with an IQR of 2.25. For multilayer clouds, the mean D_{ar} is -0.99 ± 2.40 km and the median D_{ar} is -0.73 km with an IQR of 2.69. The impact of COF on the retrieval accuracy cannot be determined because most of the comparisons with CD > 1 km also have COF greater than 0.5.

4.3 Comparison between MODIS and AHI

As just addressed, MODIS and AHI CTH data have different spatial and temporal resolutions. This section compares the MODIS CTHs, averaged using data within 2.5 and 5 km from the IAP site, with the nearest AHI CTHs, respectively. Observation time interval of comparisons is limited within 5 min. More than 600 valid comparisons are matched and are shown in Fig. 11. The mean D_{am} is -0.70 ± 2.49 km for the 2.5 km collocation and -0.64 ± 2.36 km for the 5 km collocation. The median (IQR) D_{am} is -0.45 (2.18) km for the 2.5 km collocation and -0.43 (1.93) km for the 5 km collocation. The peak D_{am} is at -0.17 km and -0.18 km, respectively. Statistically, the 5 km collocation method shows larger CTH bias than the 2.5 km collocation. These results are close to the results from Kouki et al. (2016), who reported that the mean AHI CTH was smaller than the MODIS CTH by -0.54 km based on measurements over 13 d in August. Also, the CTH difference shows an obvious relationship with COT.

Based on the analysis in Sect. 4.1–4.3, an overview of the statistical results is presented in Table 3. Statistically, MODIS CTHs and AHI CTHs are lower than radar CTHs; the median differences are closer to the peak differences than the mean differences due to the non-Gaussian distribution of difference. Note that the comparisons between MODIS and

Ka band, between AHI and Ka band, and between MODIS and AHI are based on different comparison samples. Therefore, due to lower median and peak D_{ar}, AHI CTHs are lower on average than MODIS CTHs, though the mean D_{mr} and mean D_{ar} are close to each other. It also can be found that the CTH difference between the two satellite instruments is smaller than the difference between the satellite instrument and the ground-based radar.

4.4 Seasonal variation

The monthly mean and median D_{mr} and D_{ar} are calculated and presented in Fig. 12 as a reference for the meteorological application of the CTH datasets.

Beijing is in northern China and has a typical continental monsoon climate. It is located in the subtropical monsoon zone, with southwest and southeast monsoons prevailing in summer and the northwest monsoon prevailing in winter. Rainfall is greater in summer, with less rain but more snow occurring in winter. The cloud distribution also shows strong seasonal variations. As shown in Fig. 12, the monthly variation in mean D_{ar} is greater than mean D_{mr} and shows seasonal characteristics. It is clear that the AHI CTH retrieval algorithm has lower uncertainty in summer (June–August), while it has the largest uncertainty in winter. The MODIS CTH retrieval algorithm also shows better performance in summer than in the other seasons. It is likely due to the seasonal characteristics of cloud distribution that summer has more thick clouds.

5 Summaries and discussions

The accuracy of the CTH retrieval algorithm of MODIS and AHI is associated with the instrument, such as the radiance calibration, signal–noise ratio, the spectral response function, and so on. It is also associated with the calculation accuracy of the radiative transfer model and the uncertainty caused by the theoretical assumptions. In an effort to better understand the performance of satellite CTH retrieval algorithms for Beijing, this study evaluates the accuracy of the MODIS and AHI CTH datasets with ground-based radar data based on 2 years of measurements.

Overall, the CTHs retrieved from the two passive sensors on board satellites (Aqua/Terra and HW8) are lower on average than the surface radar data. Furthermore, the retrieval accuracy strongly depends on cloud depth. As the retrieval algorithms determine that the retrieved CTH mostly represents the position of the radiation centre of the clouds, it is reasonable that most CTHs retrieved by MODIS and AHI are lower than the radar CTHs. The CTH difference between two satellite instruments is smaller than the difference between satellite instrument and ground-based radar.

It is found that retrieved MODIS CTHs greater than 6 km are closer to radar CTH than those lower than 4 km.
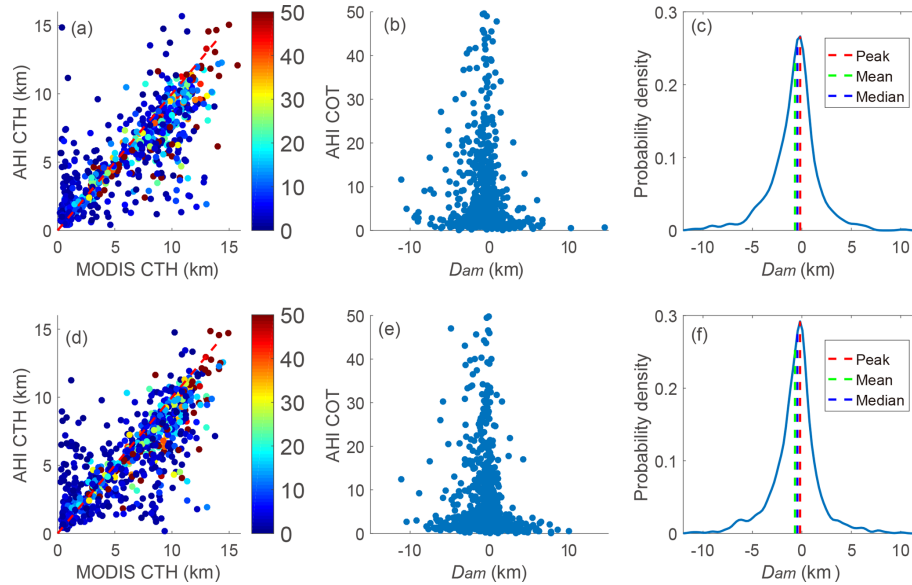
Figure 11. Statistical results of the MODIS CTHs and the nearest AHI CTHs of all comparisons. For the 2.5 km collocation, panel **(a)** is the scatter plot of all MODIS CTHs and the AHI CTHs. Panel **(b)** shows the relationship between the D_{am} and the COT. Panel **(c)** presents the probability density distribution of D_{am}, same as Fig. 9b. Panels **(d–f)** are the same as **(a–c)** but for a 5 km radius.
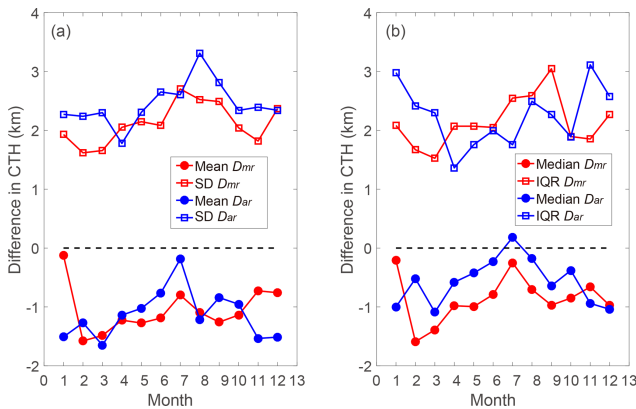
Figure 12. Monthly variations in **(a)** the mean and standard deviation of the D_{mr} and the D_{ar}, and **(b)** the median and IQR of the D_{mr} and the D_{ar}.

The large differences are mainly from high and thin clouds (CD < 1 km). In particular, retrieval differences are enlarged when the CBH is greater than 4 km. The mean D_{mr} for clouds with CD > 1 km is -0.48 ± 1.70 km and -0.29 ± 1.43 km for clouds with CD > 2 km. For the AHI, the mean D_{ar} decreases as CD increases, i.e. the mean D_{ar} is -1.52 ± 2.84 for CD < 1 km, while the D_{ar} declines to -0.76 ± 1.63 km for CD > 1 km. The median differences and IQR are also calculated to investigate the CTH difference, and it is found that those median CTH biases are smaller than the mean biases due to the non-Gaussian distribution of difference.

Statistical analysis shows that the mean AHI CTHs are lower than the MODIS CTHs over Beijing. On the basis of

2 years of data, the seasonal changes in the CTH retrieval bias for both sensors is also studied. Both MODIS and AHI retrieval algorithm have the lowest bias in summer.

This study shows the CTH retrieval accuracy of MODIS and AHI and provides a reference for a better understanding of the climatological trends of clouds based on satellite datasets and to enhance their application in GCM models. However, this study does not consider the causes of the retrieval uncertainties. By combining the results of this study with an analysis of the raw radiance data and source retrieval codes, more insights into improvement of the retrieval algorithms can be obtained in the future.

Author contributions. JH and DL designed the comparisons, and JH carried them out. SD and YB prepared the ground-based radar data. BL prepared some Himawari data and references. JH prepared the manuscript with contributions from all co-authors.

References

Ackerman, S. A., Strabala, K. I., Menzel, W. P., Frey, R. A., Moeller, C. C., and Gumley, L. E.: Discriminating clear sky from clouds with MODIS, J. Geophys. Res., 103, 32141–32157, 1998.

Arakawa, A.: The cumulus parameterization problem: Past, present, and future, J. Climate, 17, 2493–2525, 2004.

Atlas, D.: The estimation of cloud parameters by radar, J. Meteor., 11, 309–317, 1954.

Baum, B. A., Menzel, W. P., Frey, R. A., Tobin, D. C., Holz, R. E., Ackerman, S. A., Heidinger, A. K., and Yang, P.: MODIS cloud-top property refinements for Collection 6, J. Appl. Meteor., 51, 1145–1163, 2012.

Bessho, K., Date, K., Hayashi, M., Ikeda, A., Imai, T., Inoue, H., Kumagai, Y., Miyakawa, T., Murata, H., Ohno, T., Okuyama, A., Oyama, R., Sasaki, Y., Shimazu, Y., Shimoji, K., Sumida, Y., Suzuki, M., Taniguchi, H., Tsuchiyama, H., Uesawa, D., Yokota, H., and Yoshida, R.: An introduction to Himawari-8/9 – Japan's new-generation geostationary meteorological satellites, J. Meteorol. Soc. Jpn., 94, 151–183, 2016.

Boucher, O., Randall, D., Artaxo, P., Bretherton, C., Feingold, G., Forster, P., Kerminen, V., Kondo, Y., Liao, H., Lohmann, U., Rasch, P., Satheesh, S., Sherwood, S., Stevens, B., and Zhang, X. Y.: Clouds and Aerosols, in: Climate Change 2013: The Physical Science Basis, Contribution of Working Group I to the Fifth Assessment Report of the Intergovernmental Panel on Climate Change, edited by: Stocker, T. F., Qin, D., Plattner, G., Tignor, M., Allen, S., Boschung, J., Nauels, A., Xia, Y., Bex, V., and Midgley, P.: Cambridge University Press, Cambridge, United Kingdom and New York, NY, USA, 571–657, 2013.

Cess, R. D., Zhang, M. H., Zhou, Y., Jing, X., and Dvortsov, V.: Absorption of solar radiation by clouds: Interpretations of satellite, surface, and aircraft measurements, J. Geophys. Res.-Atmos., 101, 23299–23309, 1996.

Chang, F. L., Minnis, P., Ayers, J. K., McGill, M. J., Palikonda, R., Spangenberg, D. A., Smith Jr., W. L., and Yost, C. R.: Evaluation of satellite – upper troposphere cloud top height retrievals in multilayer cloud conditions during TC4, J. Geophys. Res., 115, https://doi.org/10.1029/2009JD013305, 2010.

Dong, X., Minnis, P., Xi, B., Sun-Mack, S., and Chen, Y.: Comparison of CERES – stratus cloud properties with ground – measurements at the DOE ARM Southern Great Plains site, J. Geophys. Res.-Atmos., 113, https://doi.org/10.1029/2007JD008438, 2008.

Eyre J. R.: A fast radiative transfer model for satellite sounding systems. ECMWF Technical Memoranda, available at: https://www.ecmwf.int/node/9329, 176, https://doi.org/10.21957/xsg8d92y3, 1991.

Görsdorf, U., Lehmann, V., Bauer-Pfundstein, M., Peters, G., Vavriv, D., Vinogradov, V., and Volkov, V.: A 35 GHz polarimetric Doppler radar for long-term observations of cloud parameters – Description of system and data processing, J. Atmos. Ocean. Tech., 32, 675–690, 2015.

Håkansson, N., Adok, C., Thoss, A., Scheirer, R., and Hörnquist, S.: Neural network cloud top pressure and height for MODIS, Atmos. Meas. Tech., 11, 3177–3196, https://doi.org/10.5194/amt-11-3177-2018, 2018.

Ham, S. H., Sohn, B. J., Yang, P., and Baum, B. A.: Assessment of the quality of MODIS cloud products from radiance simulations, J. Appl. Meteor., 48, 1591–1612, 2009.

Hamada, A. and Nishi, N.: Development of a cloud-top height estimation method by geostationary satellite split-window measurements trained with CloudSat data, J. Appl. Meteor., 49, 2035–2049, 2010.

Hamann, U., Walther, A., Baum, B., Bennartz, R., Bugliaro, L., Derrien, M., Francis, P. N., Heidinger, A., Joro, S., Kniffka, A., Le Gléau, H., Lockhoff, M., Lutz, H.-J., Meirink, J. F., Minnis, P., Palikonda, R., Roebeling, R., Thoss, A., Platnick, S., Watts, P., and Wind, G.: Remote sensing of cloud top pressure/height from SEVIRI: analysis of ten current retrieval algorithms, Atmos. Meas. Tech., 7, 2839–2867, https://doi.org/10.5194/amt-7-2839-2014, 2014.

Huo, J. and Lu, D.: Cloud determination of all-sky images under low-visibility conditions, J. Atmos. Ocean. Tech., 26, 2172–2181, 2009.

Huo, J., Bi, Y., Lü, D., and Duan, S.: Cloud Classification and Distribution of Cloud Types in Beijing Using Ka-Band Radar Data, Adv. Atmos. Sci., 36, 793–803, 2019.

King, M., Tsay, S., Platnick, S., Wang, M., and Liou, K.: Cloud Retrieval: Algorithms for MODIS: Optical thickness, effective particle radius, and thermodynamic phase, Algorithm Theoretical Basis Document, ATBD-MOD-05, 83 pp., 1998.

Kouki, M., Hiroshi, S., Ryo, Y., and Toshiharu, I.: Algorithm theoretical basis document for cloud top height product, Meteorolgical Satellite Center Technical Note, https://www.data.jma.go.jp/mscweb/technotes/msctechrep61-63.pdf (last access: 19 June 2019), 2016.

Liou, K. N.: Radiation and cloud rrocesses in the atmosphere: theory, observation, and modeling, Oxford University Press, 487 pp, 1992.

Marchand, R.: Trends in ISCCP, MISR, and MODIS cloud-top-height and optical-depth histograms, J. Geophys. Res.-Atmos., 118, 1941–1949, 2013.

Marchand, R., Ackerman, T., Smyth, M., and Rossow, W.: A review of cloud top height and optical depth histograms from MISR, ISCCP, and MODIS, J. Geophys. Res.-Atmos., 115, https://doi.org/10.1029/2009JD013422, 2010.

Menzel, W., Frey, R., Zhang, H., Wylie, D., Moeller, C., Holz, R., Maddux, B., Baum, B., Strabala, K., and Gumley, L.: MODIS global cloud-top pressure and amount estimation: algorithm description and results, J. Appl. Meteorol., 47, 1175–1198, 2008.

Mouri, K., Izumi, T., Suzue, H., and Yoshida, R.: Algorithm Theoritical Basis Document of cloud type/phase product, Meteorological Satellite Center, Technical Note, 61, 19–31, 2016.

Naud, C., Muller, J. P., and Clothiaux, E. E.: Comparison of cloud top heights derived from MISR stereo and MODIS CO_2, Geophys. Res. Lett., 29, 421–424, 2002.

Nieman, S. J., Schmetz, J., and Menzel, W. P.: A comparison of several techniques to assign heights to cloud tracers, J. Appl. Meteorol., 32, 1559–1568, 1993.

Pavolonis, M. J. and Heidinger, A. K.: Daytime cloud overlap detection from AVHRR and VIIRS, J. Appl. Meteorol., 43, 762–778, 2004.

Pincus, R., Platnick, S., Ackerman, S. A., Hemler, R. S., and Patrick Hofmann, R. J.: Reconciling simulated and observed views of clouds: MODIS, ISCCP, and the limits of instrument simulators, J. Climate, 25, 4699–4720, 2012.

Remer, L. A., Kleidman, R. G., Levy, R. C., Kaufman, Y. J., Tanré, D., Mattoo, S., Martins, J. V., Ichoku, C., Koren, I., Yu, H., and Holben, B. N.: Global aerosol climatology from the MODIS satellite sensors, J. Geophys. Res.-Atmos., 113, https://doi.org/10.1029/2007JD009661, 2008.

Ramanathan, V. L. R. D., Cess, R. D., Harrison, E. F., Minnis, P., Barkstrom, B. R., Ahmad, E., and Hartmann, D.: Cloud-radiative forcing and climate: Results from the Earth Radiation Budget Experiment, Science, 243, 57–63, 1989.

Rodell, M. and Houser, P. R.: Updating a land surface model with MODIS-derived snow cover, J. Hydrometeorol., 5, 1064–1075, 2004.

Roskovensky, J. K. and Liou, K. N.: Simultaneous determination of aerosol and thin cirrus optical depths over oceans from MODIS data: Some case studies, J. Atmos. Sci., 63, 2307–2323, 2006.

Rossow, W. B. and Schiffer, R. A.: Advances in understanding clouds from ISCCP, Bound.-Lay. Meteorol., 80, 2261–2288, 1999.

Schmetz, J., Holmlund, K., Hoffman, J., and Strauss, B.: Operational cloud motion winds from Meteosat infrared images, J. Appl. Meteorol., 32, 1207–1225, 1993.

Schiffer, R. A. and Rossow, W. B.: The International Satellite Cloud Climatology Project (ISCCP): The first project of the world climate research programme, Bound.-Lay. Meteorol., 64, 779–784, 1983.

Smith, W. L. and Platt, C. M. R.: Comparison of satellite-deduced cloud heights with indications from radiosonde and ground-based laser measurements, J. Appl. Meteorol., 17, 1796–1802, 1978.

Stephens, G. L. and Kummerow, C. D.: The remote sensing of clouds and precipitation from space: A review, J. Atmos. Sci., 64, 3742–3765, 2007.

Stubenrauch, C. J., Del Genio, A. D., and Rossow, W. B.: Implementation of subgrid cloud vertical structure inside a GCM and its effect on the radiation budget, J. Climate, 10, 273–287, 1997.

Wang, T., Luo, J., Liang, J., Wang, B., Tian, W., and Chen, X.: Comparisons of AGRI/FY-4A cloud fraction and cloud top rressure with MODIS/Terra measurements over East Asia, J. Meteorol. Res., 33, 705–719, 2019.

Weisz, E., Li, J., Menzel, W. P., Heidinger, A. K., Kahn, B. H., and Liu, C. Y.: Comparison of AIRS, MODIS, CloudSat and CALIPSO cloud top height retrievals, Geophys. Res. Lett., 34, https://doi.org/10.1029/2007GL030676, 2007.

Wetherald, R. T. and Manabe, S.: Cloud feedback processes in a general circulation model, J. Atmos. Sci., 45, 1397–1416, 1988.

Xi, B., Dong, X., Minnis, P., and Sun-Mack, S.: Comparison of marine boundary layer cloud properties from CERES – Edition 4 and DOE ARM AMF measurements at the Azores, J. Geophys. Res.-Atmos., 119, 9509–9529, https://doi.org/10.1002/2014JD021813, 2014.

Xiao, P., Huo, J., and Bi, Y.: Ground-based Ka- band cloud radar data quality control. Journal of Chengdu University of Information Technology, Journal of Chengdu University of Information Technology, 33, 129–136, https://doi.org/110.16836/j.cnki.jcuit.12018.16802.16005, 2018.

Zhou, Q., Zhang, Y., Li, B., Li, L., Feng, J., Jia, S., Lv, S., Tao, F., and Guo, J.: Cloud-base and cloud-top heights determined from a ground-based cloud radar in Beijing, China, Atmos. Environ., 201, 381–390, https://doi.org/310.1016/j.atmosenv.2019.1001.1012, 2019.